2012

Thermal-Hydraulic Performance of Metal Foam Heat Exchangers

Kashif Nawaz
nawaz1@illinois.edu

Jessica Bock

Anthony M. Jacobi

Thermal-Hydraulic Performance of Metal Foam Heat Exchangers

Kashif NAWAZ [1]*, Jessica BOCK[1], Anthony JACOBI[1]

[1]University of Illinois at Urbana-Champaign, Department of Mechanical Science and Engineering

Urbana, IL, 61801 USA

+1 217 377-1528, nawaz1@illinois.edu

ABSTRACT

Due to their large surface-area-to-volume ratio and tortuous structure, metal foams hold promise for heat transfer applications. Both of these factors increase the heat transfer by enhancing the mixing and surface area. The main disadvantage associated with their thermal-hydraulic performance is relatively higher pressure drop, resulting in larger pumping power requirements if they are used in a heat exchanger. In this paper, open-cell aluminum metal foam is considered as a highly compact replacement for conventional fins in brazed aluminum heat exchangers. SEM techniques are used to characterize the foam characteristics such as pore and ligament diameter. Experiments are conducted by a closed-loop wind tunnel to measure the pressure drop and heat transfer rates. The effects of different porosity, fin depth, bonding method, base metal, condensation and frost are considered. It is found that incorporating foam with smaller pores results in larger pressure drop per unit length but the heat transfer rate is higher as well. Fin depth can be changed as well to reduce the pressure drop. Furthermore, metal foams, found to perform much better compared to other designs employing plain fins or louver fins with much larger heat transfer coefficients. Permeability and inertia coefficients are determined and compared with the reported data. An appropriate length scale is suggested for the data reduction. Based on the experimental findings, a model has been developed relating the foam characteristics and flow conditions to the pressure drop and heat transfer.

1. INTRODUCTION

Metal foams appear to have attractive properties for heat transfer applications and have been used for thermal applications in cryogenics, combustion chambers, geothermal systems, petroleum reservoirs, catalytic beds, compact heat exchangers for airborne equipment, air-cooled condensers and compact heat sinks for power electronics. The foam provides an extended surface with high surface area and complex flow paths. That combination is expected to yield excellent convective heat transfer performance. Typically, increased compactness (higher heat transfer surface area per unit volume) leads to an increase in pressure drop per unit flow length. Metal foam heat exchangers have very high surface-area-to-volume ratios and are thus anticipated to have relatively large pressure drop per unit length. This expectation is reinforced by the complex geometry of the foams which results in a high degree of boundary layer restarting and wake destruction by mixing. If metal foams are to be widely used in thermal systems, their pressure-drop and heat transfer characteristics must be available to potential users in terms that fit into current design methods. Metal foams are characterized by the size of the windows (or pore diameter) which correlates with the nominal pore density (PPI), the strut diameter and length, and the porosity ε (volume of void divided by the total volume of the solid matrix and void). Although there have been numerous recent reports on metal-foam heat transfer during single phase flow in foams, to date there is no general model available for thermal-hydraulic performance of metal foams, and researchers must rely on experimental data. This paper focuses on the experimental analysis of heat transfer during air flow in aluminum foams with different number of pores per inch, different geometry and different base metals.

2. LITERATURE REVIEW

Metal foams are a relatively new class of materials with low densities and novel thermal, mechanical, and acoustic properties. They were initially developed in 1960s by the US Navy for cooling inter-ballistic missile components and were maintained under secrecy until the early 1980s when they became commercially available in the US. The recent development of a variety of processes for producing them at lower cost, yet with improved properties, has increased their applications (Zhou *et al.*,2002). They have been used in aerospace applications (Ashby *et al.*,2000), geothermal operations, and petroleum processing (Vafai and Chen, 1982). Aluminum has emerged as the prime material for metal foams due to its low density, high thermal conductivity, and its relatively low price. Extensive

reviews of the topic of fluid flow in porous media in general can be found in (Kaviany, 1995). The porous matrix of metal foam consists of tortuous irregularly shaped flow passages with a continuous disruption of hydrodynamic and thermal boundary layers. The flow recirculates at the back of the solid fibers, and turbulence and unsteady flows often occur (Bastawros *et al.*, 1998).

Decker *et al.* (2000) provided detailed experimental characterization and numerical modeling of the heat and mass transport in highly porous nickel-chromium alloy foam. Tadrist *et al.* (2004) investigated the use of aluminum foam for compact heat exchangers. Kim *et al.* (2000) carried out systematic experiments to study the friction and the heat transfer characteristics of porous fins in a plate-fin heat exchanger using water. Bhattacharya *et al.* (2002) provided analytical and experimental results for the permeability and the friction coefficient for aluminum foam. Du Plessis *et al.* (1994) provided a geometrical model for the fluid dynamics in metal foams. Boomsma and Poulikakos (2002) measured the hydraulic and thermal performance of open-cell, 40 PPI aluminum foam, compressed and uncompressed, with porosities between 60.8 and 88.2%.

Hsieh *et al.* (2004) carried out an experimental study to characterize the heat transfer behavior of several heat sinks made of aluminum metal foams. Kim *et al.* (2000) measured the heat transfer coefficient for air flowing through aluminum foams. Giani *et al.* (2005) presented experimental interstitial heat transfer coefficients, measured for FeCr Alloy and Cu foams with 5.4, 5.6 and 12.8 PPI, by performing transient cooling experiments with air. Hwang *et al.* (2002) measured interstitial convective heat transfer coefficients for air flowing in 10 PPI aluminum foams with porosities of 0.7, 0.8, 0.95, applying a transient single-blow technique. Kim *et al.* (2001) measured the heat transfer coefficient with air flowing in three aluminum foams with 10, 20, 40 PPI and a fixed porosity ε=0.92. Younis and Viskanta (1993) presented an experimental investigation to characterize the volumetric heat transfer coefficient between a heated air stream and ceramic foams (alumina and cordierite). Dukhan and Chen (2007) presented heat transfer measurements inside rectangular blocks of commercially available aluminum foam subjected to constant heat flux at one side, cooled by air. Boomsma and Poulikakos (2002) measured the hydraulic performance of compressed and uncompressed aluminum foams using water with a maximum frontal velocity (Darcy velocity) of 1.4 m/s. Dai *et al.* (2010) reviewed the mechanistic basis of the Boomsma-Poulikakos model and provided an extension to the approach to account for ligament orientation. They also compared the heat transfer and pressure drop performance of metal-foam heat exchangers to another state-of-the-art heat exchanger (Dai *et al.* 2012). Nawaz *et al.* (2010) considered open-cell aluminum metal foam as a highly compact replacement for conventional fins in brazed aluminum heat exchangers. Moffat *et al.* (2009) showed that three parameters must be known to calculate the heat transfer performance of a foam-fin: the convective conductance per unit volume, the effective conductive conductance as a fin, and the effective thermal resistance between the foam and the surface to which it was attached.

3. EXPERIMENTAL METHODS

3.1 Experimental apparatus

Dry and wet wind tunnel testing was conducted using a closed-loop wind tunnel for thermal hydraulic performance tests. As shown in Figure.1a, air downstream of test section passed through a set of electric strip heaters, past a steam injection pipe, through an axial blower and another set of strip heaters, a flow nozzle, a mixing chamber, a flow conditioning section, a flow contraction, and the test section, completing the loop. Heater-controllers were used to maintain the desired upstream air temperature and dew point at steady state. Steam was generated by an electric humidifier. The air temperature was measured using thermocouple grids, constructed using T-type thermocouples (4 channels upstream; 9 channels downstream), and chilled-mirror hygrometers were used to measure the upstream and downstream dew points. The cross-sectional flow area in the test section was rectangular, 30 cm wide and 20 cm high. An axial blower provided an air flow with face velocities at the test section from 0.3 to 7 m/s. An ASME flow nozzle, with a differential pressure transducer, was used to measure air mass flow rate. Another pressure transducer was used to measure air-side pressure drop across the test section. A single-phase liquid, an aqueous solution of Ethylene Glycol (DOWTHERM 4000), was used as the tube-side heat transfer fluid. A chiller system with a commercial heat pump, two large coolant reservoirs, a PID-controlled electric heater, and a gear pump supplied the flow. The chiller system provided a coolant flow with a steady inlet temperature (within 0.1°C) at a capacity up to 20 kW. Coolant inlet and outlet temperatures were measured using RTDs with an uncertainty less than 0.05°C. A coriolis-effect flow meter located in the downstream coolant pipe was used to measure mass flow rate. A PC-based data acquisition system (National Instruments) was used to record and monitor the experimental data. The significant experimental uncertainties involved in the dry and wet wind-tunnel experiments are listed in Table 1.

Before beginning wind-tunnel tests, the heat exchanger specimens were insulated using foam insulation tape. The specimens were mounted in the test section, the coolant hoses connected, and the gaps between the specimen and the test section sealed with adhesive tape. The entire wind tunnel, the test specimen, steam pipes, and coolant pipes were all insulated to isolate the system from the environment. Once the installation was complete, the components of the test apparatus were started and set to the desired test point temperatures, dew point, and flow rates. Steady-state conditions were considered to prevail when all individual variables measured were maintained constant within instrument uncertainty. The recorded parameters include upstream and downstream air temperature, upstream and downstream dew point, coolant inlet and outlet temperature, nozzle pressure drop, core pressure drop, coolant mass flow rate, nozzle upstream pressure, ambient barometric pressure, and ambient air temperature. The data stream was sampled for a period long enough to ensure that the averaged readings were independent from temporal fluctuations (i.e., independent form random instrument errors). All experiments had an energy balance within 10%.

3.2 Sample manufacturing

Metal foam heat exchangers were built in different confrigurations. In total 16 heat exchnagers were tested for the thermal-hydraulic performacne analysis. Three different methods were used to join the foam with the tubes including thermal epoxy, Artic silver 5, and brazing. Figure.1b shows a representative sample with the 10 PI metal foam. Samples to compare the effect of pore size were prepared with same confriguration while deploying foams with different pore sizes (5,10,20 and 40 PPI). Specifications and dimensions shown of samples are representaed in Table 1, and the test conditions are summarized in Table 2.

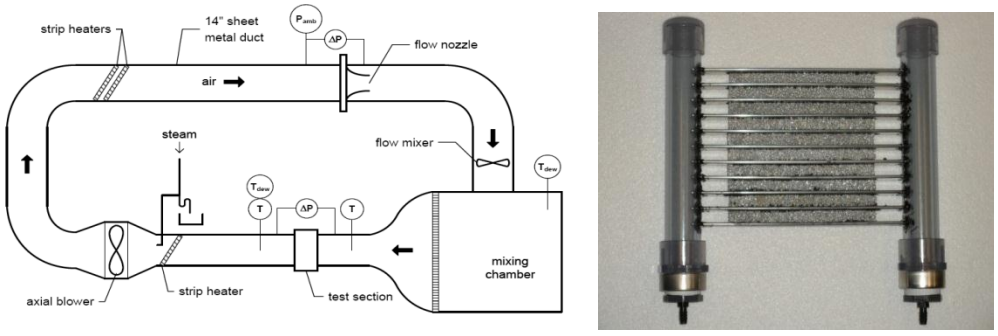

(a) (b)

Figure 1: (a) Wind tunnel apparatus, (b) flat tube metal foam heat exchanger (10 PPI metal foam)

Table 1: Design specifications and dimensions of heat exchangers

Base metal	Al 6061 alloy
Porosity	5,10,20,40 PPI
Tube side configuration	Micro channel flat tube (1.5 mm * 1.5 mm) 8 channels
Number of fins	10
Fin depth	15 mm
Fin thickness	15 mm
Bonding method	Artic silver, thermal compound, Brazed
Face area	200 mm×174 mm
Tube width	25.4 mm
Tube wall thickness	0.5 mm

Table 2: Experimental conditions

Test condition	Coolant flow rate (Kg/sec)	Inlet coolant temperature (^{0}C)	Inlet air temperature (^{0}C)	Inlet humidity (%)
Dry	0.082±0.001	8±3	33±5	60

3.3 Data reduction

The total rate of heat transfer, q, is determined from an energy balance on each stream, and the modeling relies on an overall approach, as does all the prior work cited. Namely, for a metal foam heat exchanger operating under dry-surface conditions:

$$q = UA \cdot LTMD \tag{1}$$

$$LMTD = F \frac{(T_{air,in} - T_{coolant,out}) - (T_{air,out} - T_{coolant,in})}{\ln\left(\frac{T_{air,in} - T_{coolant,out}}{T_{air,out} - T_{coolant,in}}\right)} \tag{2}$$

LMTD is determined from the measured temperatures, with the flow configuration factor, F, from Incropera and Dewitt (2006). The overall thermal conductance of the heat exchanger, UA, is formulated by neglecting the conduction resistance of the tube wall:

$$\frac{1}{UA} = \left(\frac{1}{\eta_o Ah}\right)_{air} + \left(\frac{1}{Ah}\right)_{coolant} + R_{bond} \tag{3}$$

The coolant-side convection coefficient is determined for the in-tube single-phase flow during the experiments, based on the geometry and flow, and there are no coolant-side fins. The thermal contact resistance due to bonding the foam to the tubes, R_{bond}, is determined from ancillary experiments described later. The air-side fin effect is accounted for using the surface efficiency

$$\eta_o = 1 - \frac{A_{foam}\left(1 - \eta_f\right)}{A_{foam} + \varepsilon A_{base}} \tag{4}$$

The surface area of the foam for air-side convection, A_{foam}, is determined from manufacturer's data for foam surface area per unit volume, using a volume of the base area, A_{base} times a fin height, L_f. The fin height, L_f, is taken as half the tube spacing. The fin efficiency is then calculated assuming a straight fin with an adiabatic tip.

$$\eta_f = \frac{\tanh(m_{foam} L_f)}{m_{foam} L_f} \tag{5}$$

where the fin parameter accounts for the ligament and pore diameters, D_f and D_p, respectively

$$m_{foam} = \sqrt{3\pi D_f h / (D_p^2 k_{eff})} \tag{6}$$

and the effective thermal conductivity of the foam is taken as the solid-only effective thermal conductivity.

$$k_{eff} = (1 - \varepsilon) k_{solid} / 2 \tag{7}$$

4. EXPERIMENTAL RESULTS

The results for the pressure drop per unit length are plotted against the face velocity under dry surface conditions in Figure 2. As demonstrated by the figure, the pressure drop per unit length increases with an increase in PPI (a decrease in pore size). The 5 PPI foam, with a pore size of about 4 mm, showed the smallest pressure drop for all face velocities, while the 40 PPI foam, with pore size of about 1.8 mm resulted in the highest pressure drop. Another interesting finding is how the pressure gradient depends on pore size. The pore size differed by about 30% between the 5 PPI and 10 PPI foams, and the pressure gradient increased by roughly 15 to 20 percent at high velocities. At velocities below about 3 m/s, the difference was negligible. However when the pore size becomes smaller the pressure gradient showed an obvious difference even for small face velocities, as can be observed in Figure 2. While reducing the data for the pressure gradient, the effect of flat tubes between metal foam fins was neglected, their contribution to pressure drop was very small compared to the porous metal foam. The heat transfer rate depends on the surface area of the metal foam. Larger heat transfer is possible if the surface area per unit volume is high. The effect of porosity (pore density in PPI) on the air-side heat transfer is also presented in Figure 2. The 40 PPI foam showed the largest heat transfer rate under all face velocities due to having the highest surface area to volume ratio, while the 5 PPI foam had the smallest heat transfer rate. It is not only surface area which contributes to larger heat transfer rate. Small pore diameters imply more ligaments per unit volume, and more ligaments promote flow mixing.

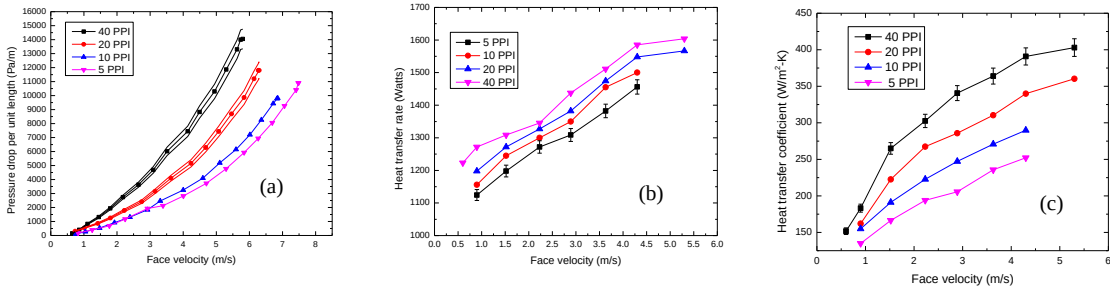

Figure 2: Thermal-hydraulic data for aluminum metal foams (a) pressure gradient, (b) heat duty, (c) heat transfer coefficient.

4.1 Geometry of heat exchanger

Seeking an improvement in the press-drop performance of metal foams, alternate geometric deployments of the metal foam were explored. In undertaking new deployments, face area, volume, and mass can be constraints. There were two round-tube heat exchangers used in this comparison, and they had identical face areas and flow depths. *Sample 1* had a continuous block deployment of foam, with round tubes running through the foam block. *Sample 2* had an annular metal foam layer on the round tubes (Figure 3). The pressure drop data for the two round-tube foam heat exchangers are presented in Figure 4. It is obvious that the sample with a continuous metal foam block had a higher pressure drop compared to the annular foam configuration. There was almost no difference in the heat transfer performance of these heat exchangers (Figure 4).

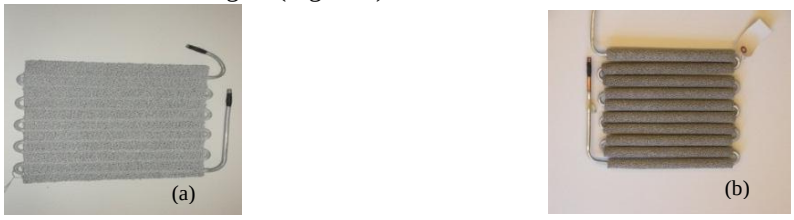

Figure 3: Metal foam heat exchangers with different geometry (a) Sample 1-continuous block (b) Sample 2-Annulur

These comparisons show that the higher pressure drop associated with metal foams can be mitigated by judicious deployment of the metal foam, so that the heat transfer performance remains excellent, and the fan power requirements are reduced.

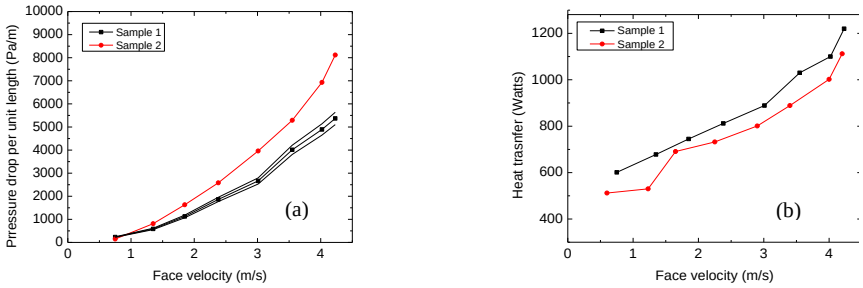

Figure 4: Pressure drop per unit length for foams of different geometry

4.2 Effect of flow depth

In order to explore the effect of flow depth, or flow development, on the pressure drop, experiments were conducted for varying test specimen thickness. As can be seen from Figure 5, pressure drop per unit length is constant for the extremes in pore size, the 5 PPI and 40 PPI metal foams, over the range of flow depths considered. The results ensure that, although the pressure drop per unit length depends on the type of foam, the effect of flow depth can be neglected, as the pressured drop per length is almost constant for these flow depths. The data suggest that the flow essentially reaches a fully developed condition in these aluminum foams.

4.3 Effect of bonding method

Thermal performance of metal foam depends on the contact resistance between the base surface (tube) and the metal foam fins. The bonding technique can greatly affect the heat transfer rate. Three different bonding methods were used to join the metal foam between flat tubes or micro-channel tubes. Experiments were conducted with samples having same geometry but different joining methods. A comparison based on the total air side resistance is presented in Figure 6. Artic silver epoxy and thermal compound have thermal conductivity of 5 W/(m·K) and 3.5 W/(m·K), respectively. With R_{bond} from these ancillary experiments, and the tube-side resistance taken from well-established correlations, it was possible to isolate the air-side convective resistance.

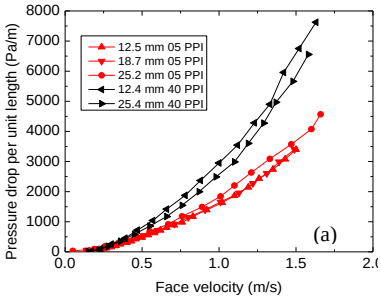

Figure 5: Flow depth effects on pressure gradient

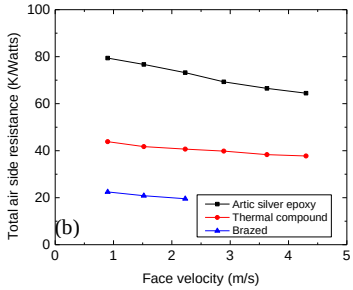

Figure 6: Bonding effects on air-side thermal resistance

4.4 Effect of base metal

Although the focus of this work is on aluminum metal foams, it is well known that the thermal conductivity of the base metal affects the foam thermal conductivity. In order to explore this effect, two samples of the same geometry with differing base metals were constructed (frontal area, flow depth, number of tubes, *etc*; see Figure 7). The thermal performance of two heat exchangers is compared in Figure 7.

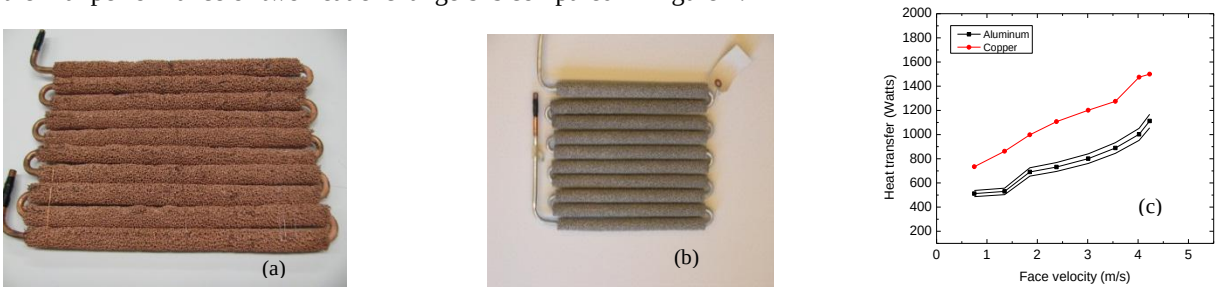

Figure 7: Metal foam heat exchangers with different base material, (a) copper and (b) aluminum, and (c) their heat transfer rates

The copper sample was constructed with copper tubes through annular copper foam, while the aluminum sample had aluminum tubes and foam and was of essentially the same geometry. The copper sample showed much better performance, as the heat transfer rate was increased by almost 50%. For both samples the heat transfer rate increased as the face velocity increased, and the rate of increase was almost same. This behavior supports the idea that the only difference between the performances of two samples is due to the differences in thermal conductivity. The thermal hydraulic performance of copper foam heat exchanger is affected by the porosity and geometry in roughly the same way as for the aluminum foam.

5. MODELING OF THERMAL HYDRAULIC PERFORMANCE

5.1 Determination of permeability and inertia coefficient

Based on the modified Darcy Flow model, the pressure gradient can be related to the hydraulic characteristics of the foam by the relation involving permeably and inertia coefficient.

$$\frac{\Delta P_f}{L} = \frac{\bar{\mu}}{K} V + \bar{\rho} C V^2 \tag{8}$$

The permeability is K, and C, is the inertia coefficient. The average viscosity and density of fluid are $\bar{\mu}$ and $\bar{\rho}$, respectively. The average properties are based on the conditions upstream and downstream of test section. This relation can be rearranged as

$$\frac{\Delta P_f}{LV} = \frac{\bar{\mu}}{K} + \bar{\rho}CV \quad (9)$$

The form of Equation (9) provides a linear relationship in face velocity

$$\frac{\Delta P_f}{LV} = A + BV \quad (10)$$

$$A = \frac{\bar{\mu}}{K} \ , B = \bar{\rho}C \quad (11)$$

These relations for *A* and *B* were used to determine the permeability and inertia coefficient for three different types of porous media. The resulting reduced pressure drop (pressure gradient divided by face velocity) was plotted against the face velocity and a linear fit provided *A* and *B*, and thus *K* and *C*. The results are summarized and compared to values from the literature in Table 4.

The values from experiments are of the same order of magnitude as those from the literature, but there are significant discrepancies. Nevertheless, the final fit to pressure gradient has a correlation coefficient of R^2=0.99792. Thus, the parameters given in Table 4 can be used with Equation (8) to obtain good fits to the current data. However, a more general approach is explored in the next section.

Table 4: Permeability and inertia coefficient for porous media*

Porous media	K_{exp}	C_{exp}	$K_{Literature}$	$C_{Literature}$
5 PPI Al	3.792(10^{-7})	0.132	2.70(10^{-7})	0.097
10 PPI Al	2.722(10^{-7})	0.095	1.49(10^{-7})	0.07
20 PPI Al	8.369(10^{-8})	0.082	1.42(10^{-7})	0.10
40 PPI Al	6.906(10^{-8})	0.086	5.68(10^{-8})	0.0899

* $K_{Literature}$ and $C_{Literature}$ are taken from Bhattacharya *et al.* (2002).

5.2 Data reduction for determination of *f* and *j* factor

For comparison purposes, the pressure-drop performance of the metal foam heat exchangers is presented following the convention of Kays and London, wherein the friction factor is related to the Reynolds number based on hydraulic diameter. With some as yet determined length scale, L_c, as an additional characteristic length and $\bar{\rho}$ the average density. The relationship for friction factor can be represented as

$$f_{Lc} = \frac{\Delta P}{L}\frac{\bar{\rho}}{G^2}\frac{L_C}{2} \quad (12)$$

where G mass flux, $G = \bar{\rho}V_{max}$ with $V_{\max}$ the velocity at the minimum free-flow area:

$$A_{min} = \sigma A_{fr} \quad (13)$$

For metal foam, the minimum free flow area, $A_{\min}$, is related to the frontal area directly by the porosity, $\sigma = \varepsilon$.
The characteristic length, L_c, can be defined by many ways. Some of the options follow:

- Heat exchanger characteristics: hydraulic diameter, flow depth, tube spacing
- Foam characteristics: pore diameter, ligament diameter, ligament length

The hydraulic diameter follows convention:

$$D_h = \frac{4A_{min}L_c}{A_T} \quad (14)$$

$$A_T = A_{foam} + A_{base} \quad (15)$$

The total surface area, A_T, is comprised of the exposed tube area, A_{base}, and the surface area of the metal foam, A_{foam}. Again, if D_h is used as L_c in Eq. (12), then the conventional definitions of Kays and London prevail, and we expect f=fncn(Re_{Dh}). In the approach embodied in Eqs (12) to (15), that convention need not be followed. However, the geometric parameters must be known.

In order to determine A_{min}, image processing was used, rather than simply relying on the reported porosities. Images from X-ray tomography were analyzed as suggested in Figure 8. In order to identify the metal in the cross sectional view of foam, a pixel threshold value of 100 was set, with pixel values ranging from 0 (black) to 255 (white). The number of pixels exceeding this threshold divided by the total gave A_{min}/A_{fr}. The process was repeated for five images for each type of foam and the values were averaged. The results are given in Table 5.

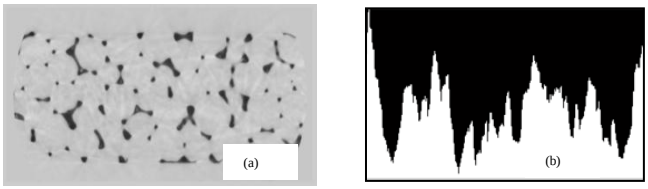

Figure 8: Image processing for cross sectional view of 5 PPI metal foam (a) X-rays image of foam slice (b) intensity distribution of the image.

Table 5: Free-flow cross-sectional area of metal foams*

Foam	Measured A_{min}/A_{fr}	Pore diameter, D_p (mm)	Ligament diameter, D_f (mm)	Hydraulic diameter, D_h (mm)
5 PPI	0.988	4.02	0.50	6.34
10 PPI	0.977	3.28	0.45	4.61
20 PPI	0.971	2.58	0.35	2.69
40 PPI	0.957	1.80	0.20	1.74

For comparison to other heat exchangers, the friction factor is plotted versus *Re* for various foams, with L_c=D_h, in Figure 9. Comparing to the general trends in Kays and London, it is clear that the metal foams have a very high *f*-factor, in the conventional sense. Moreover, because the data do not collapse to a single curve, there is a strong suggestion that another length scale is important (not simply D_h).

Through a trial and error process, it was found that the friction factor data would collapse to a single curve, with a goodness of fit suitable for engineering design, if pore diameter was included as a characteristic length. In this process 2 of 64 data were discarded as outliers; the resulting fit had a relative RMS deviation of ±14.86%, and almost all of the data were predicted to within ±20%. The fit uses pore diameter as L_c, with the Reynolds number based on hydraulic diameter

$$f_{D_p} = \frac{\Delta P}{L}\frac{\bar{\rho}}{G^2}\frac{D_p}{2} = 1.975 Re_{D_h}^{-0.1672}\left(D_p/D_h\right)^{-3.708} \qquad (16)$$

In order to facilitate comparison to conventional compact heat exchangers, the Colburn *j* factor, with L_c=D_h, is presented in Figure 9. As shown in the figure, foams with higher pore density (PPI) had higher *j* factors. In comparison to most convention heat exchangers (e.g., louvers), metal foams have a high Colburn *j* factor. Attempting to fit the data in this format only to Re_{Dh} results in fits with a relative RMS deviation of more than ±10%; however, when pore diameter, D_p, is used as an additional characteristic length, the following fit predicts all dry-foam heat transfer data with a relative RMS deviation of ±4%:

$$j_{D_p} = \frac{h}{\bar{\rho}\bar{c_p}V}\frac{D_p}{D_h}Pr^{2/3} = 2Re_{D_h}^{-0.5611}\left(D_p/D_h\right)^{0.3213} \qquad (17)$$

The predicted and measured Colburn j factors are presented in Figure 10. The relative RMS deviation is ±14.86%; and 4% and limits of ±20% and 12.5% are shown in the plot for *f* and *j*, respectively.

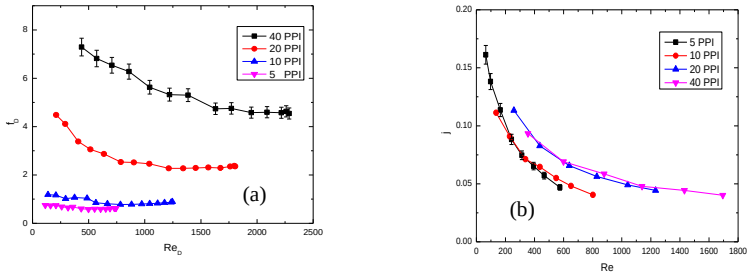

Figure 9: Thermal-hydraulic performance in terms of the conventional length scale, (a) friction factor, (b) Colburn *j* factor.

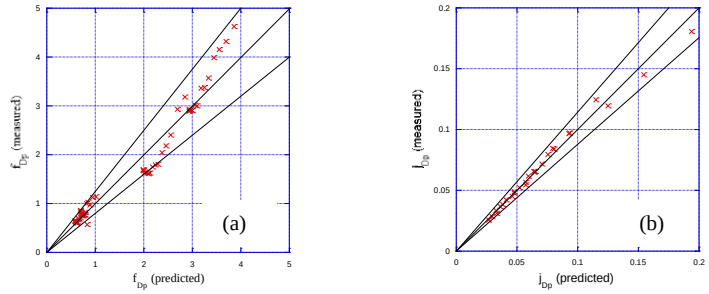

Figure 10: Thermal-hydraulic performance in terms of the alternative length scales from Equations (16) and (17), (a) friction factor, (b) Colburn *j* factor.

6. CONCLUSION

The thermal-hydraulic performance of the metal foams heat exchangers has been analyzed. It is clear that pore diameter is an important parameter in determining the pressure drop and heat transfer rate. Both pressure drop and heat transfer rate increase as the face velocity increases. The geometry of metal foam heat exchangers can considerably reduce the pressure drop without compromising the heat transfer performance. It was found that more than one length scale is important to the pressure drop and heat transfer in metal foams. The thermal-hydraulic performance of metal foam heat exchangers was better than the louver-fin heat exchanger for geometrically similar samples. There are various models available to predict the pressure gradient and heat transfer coefficient, but they are based on non-realistic geometries, and they fail to predict the performance accurately. By using a Reynolds number based on hydraulic diameter, curves fits for the friction factor and for Colburn *j* factor based on pore diameter were developed with reasonable engineering accuracy.

NOMENCLATURE

A_{fr}	Frontal area (m^2)	h	Heat transfer coefficient (W/m^2-K)
A_{min}	Minimum flow area (m^2)	j	Colburn j factor
C	Inertia coefficient	K	Permeability
D_P	Pore diameter (m)	V	Face velocity (m/s)
D_f	Ligament diameter (m)	$\Delta P/L$	Pressure drop per unit length (Pa/m)
f	Friction factor	Re_K	Reynolds number based on permeability

ACKNOWLEDGEMENT

Financial support for this project was sponsored by ARTI under project number ARTI 06030-01. We also gratefully acknowledge support from Creative Thermal Solutions (CTS), 2209 North Willow Road, Urbana IL, 61802 for providing the brazed metal-foam heat exchangers, without which, it would have been impossible to isolate the bonding/contact resistance.

REFERENCES

Ashby, M.F., Evans, A.G., Fleck, N.A., Gibson, L.J., Hutchinson, J.W., Wadley, H.N.G.,2000, Metal Foams, a Design Guide, Butterworth- Heinemann, Woburn, MA , Chap. 1: pp. 181–188.

Bastawros, A.F., Evans, A.G., Stone, H.A., 1998, Evaluation of cellular metal heat transfer media, MECH 325, Harvard University Report, Cambridge, MA.

Bhattacharya, A., Calmidi, V.V., Mahajan, R.L., 2002, Thermo-physical properties of high porosity metal foams, *International. Journal of Heat and Mass Transfer*, vol. 45:p. 1017–1031.

Boomsma, K., Poulikakos, D., 2002, The effect of compression and pore size variations on the liquid flow characteristics in metal foams, *ASME Journal of Fluids Engineering*, vol. 124:p. 263–272.

Decker. S, Mößbauer. S, Nemoda. D.T, Zapf. T, 2000, Detailed experimental characterization and numerical modeling of heat and mass transport properties of highly porous media for solar receivers and porous burners, Lehrstuhl für Strömungsmechanik Universität Erlangen-Nürnberg Cauerstr. 4, D-91058 Erlangen, Germany.

Dukhan, N., Chen, K.C., 2007, Heat transfer measurements in metal foam subjected to constant heat flux, *Experimental Thermal Fluid Science*, vol. 32: p. 624–631.

Du Plessis, J.P., Montillet, A., Comiti, J., Legrand, J., 1994, Pressure drop prediction for flow through high porosity metallic foams, *Chemical Engineering Science*, vol. 49:p. 3545–3553.

Giani, L., Groppi, G., Tronconi, E., 2005, Heat transfer characterization of metallic foams, *Industrial Chemical Engineering*, vol. 44: p. 9078–9085.

Hwang, J.J., Hwang, J.G., Yeh, R.H., Chao, C.H., 2002, Measurement of interstitial convective heat transfer and frictional drag for flow across metal foams, *ASME Journal of Heat Transfer*, vol. 124: p. 120–129.

Hsieh, W.H., Wu. J.Y., Shih, W.H., Chiu, W.C., 2004, Experimental investigation of heat transfer characteristics of aluminum-foam heat sink, *International Journal of Heat and Mass Transfer*, vol. 47:p. 5149–5157.

Incropera, F.P., DeWitt, D. P., 1996, Fundamentals of heat and mass transfer, 4th ed., John Wiley & Sons, Inc.

Kaviany, M., 1995, Principles of Heat Transfer in Porous Media, Springer-Verlag, New York, Chapter. 2.

Kim, S.Y., Paek, J.W., Kang, B.H., 2000, Flow and heat transfer correlations for porous fin in a plate-fin heat exchanger, ASME Journal of Heat Transfer, 122:p. 572–578.

Kim, S.Y., Kang, B.H., Kim, J.H., 2001, Forced convection from aluminum foam materials in an asymmetrically heated channel, *International Journal of Heat and Mass Transfer*, vol. 44: p. 1451–1454.

Moffat, R.J., Eaton, J.K., Onstad, A., 2009, A method for determining the heat transfer properties of foam-fins, *ASME Journal of Heat Transfer*, vol. 13: p. 011603-1.

Nawaz, K., Bock, J., Jacobi, A.M., 2010, Experimental studies to evaluate the use of metal foams in highly compact air-cooling heat exchangers, 13th International Refrigeration and Air Conditioning Conference, Purdue University Lafayette, IN.

Park, Y., Jacobi, A.M., 2009, Air-side heat transfer and friction correlations for flat-tube, louver-fin heat exchangers, *ASME Journal of Heat Transfer*, vol.131: p. 061801-1

Tadrist, L., Miscevic, M., Rahli, O., Topin, F., 2004, About the use of fibrous materials in compact heat exchangers, *Experimental Thermal-Fluid Science*, vol. 28:p.193–199.

Vafai, K, Chen, T.L., 1982, Boundary and inertia effects on convective mass transfer in porous media, *International Journal of Heat and Mass Transfer*, vol. 25,:p 1183–1190.

Younis, L.B., Viskanta, R., 1993, Experimental determination of the volumetric heat transfer coefficient between stream of air and ceramic foam, *International Journal of Heat and Mass Transfer*, vol. 36: p. 1425–1434.

Zhengshu, D., Nawaz, K., Bock, J., Jacobi, A.M., 2010, Correcting and extending the Boomsma-Poulikakos effective thermal conductivity model for three-dimensional, fluid-saturated metal foams, International Communications in Heat and Mass Transfer, vol. 37:p. 575-580.

Zhengshu, D., Nawaz, K., Park, Y., Chen, Q., Jacobi, A.M., 2012, A comparison of metal-foam heat exchangers to compact multi-louver designs for air-side heat transfer applications, *Heat Transfer Engineering*, vol. 33: p. 21-30.

Zhou, J., Mercer, C., Soboyejo, W.O.,2002, An investigation of the microstructure and strength of open-cell 6010 aluminum foam, *Metallurgical and Material Transactions* , vol. 33:p.1413–1427.